

# Generic reduction theory for Fermi sea topology in metallic systems

Wei Jia\*

Key Laboratory of Quantum Theory and Applications of MoE, Lanzhou Center for Theoretical Physics, and Key Laboratory of Theoretical Physics of Gansu Province, Lanzhou University, Lanzhou 730000, China

Fermi sea in a metal can host exotic quantum topology, which determines its conductance quantization and is characterized by Euler characteristic  $\chi_F$ . Unlike gapped band topology described by the global feature of wave function, this topology of gapless system is associated with the geometry of Fermi sea, and thus probing and identifying  $\chi_F$  are inherently difficult in higher-dimensional metallic systems. Here, we propose a dimensional reduction theory for Fermi sea topology in  $d$ -dimensional metallic systems, showing that  $\chi_F$  can be determined by the feature of so-called reduced critical points on Fermi surfaces, with theoretical simplicity and observational intuitiveness. We also reveal a nontrivial correspondence between the Fermi sea topology and the gapped band topology by using an ingenious mapping, of which  $\chi_F$  exactly equals to the topological invariant of gapped topological phases. This provides a potential way to capture  $\chi_F$  through the topological superconductors. Our work opens an avenue to characterize and detect the Fermi sea topology using low-dimensional momentum information.

*Introduction.*—Since the discovery of two-dimensional (2D) integer quantum Hall effect [1], quantum topology has played an important role in condensed matter physics. A most fundamental phenomenon of topological quantum phases is quantized response [2]. The quantization is associated with the global feature of wave function across the Brillouin zone, determined by defining topological invariant of the ground state [3, 4]. In metals, there is another quantum topology that significantly impacts the quantized response [5–8], which is dictated by the geometry of Fermi sea. Although this conductance quantization is not as robust as Hall conductance, it has been observed in quantum point contacts [9], semiconductor nanowires [10, 11], and carbon nanotubes [12]. There is a fundamental issue of how to exactly characterize this Fermi sea topology.

A recent breakthrough has elucidated that Fermi sea topology is characterized by Euler characteristic  $\chi_F$  [13]. This remarkable discovery provides a novel insight for understanding the quantization of conductance in metals. Various probing schemes of  $\chi_F$  but in 2D systems have also been proposed, such as multipartite entanglement [14], Andreev state transport [15, 16], and density correlations of Fermi gas [17]. The quantized response may be possible to be measured in an ultracold atomic gas [18, 19]. Nevertheless, the observation of  $\chi_F$  remains challenging in a general  $dD$  metallic system. The reason is that  $\chi_F$  is associated with the properties of filled bands, which are not easily captured for the higher-dimensional systems. There is an urgent need to develop a simpler characterization of  $\chi_F$  and facilitate its detection.

The Fermi sea topology and the gapped band topology have different topological origins, but there seems to be subtle connection between them. A simple example is that the single filled band can host a nontrivial  $\chi_F$  and the electrons on Fermi surfaces (FSs) can interact to produce Cooper pairs, thereby inducing topological superconductors (SCs) [20]. The numbers of Majorana

edge states in topological SCs is related to the Fermi sea topology of the normal filled band [21, 22]. It is interesting and necessary to reveal the connection between the topological SC and  $\chi_F$  of its normal filled band, which may promote the discoveries of other novel physical effects caused by the Fermi sea topology.

In this Letter, we propose a generic reduction theory for the Fermi sea topology in metals, of which  $\chi_F$  is determined by the features of reduced critical points which are discrete momentum points on the FSs. This characterization using lower-dimensional momentum information has theoretical simplicity and observational intuitiveness. We also demonstrate that the metallic systems can be equivalently mapped to the gapped topological systems, inducing a striking result that  $\chi_F$  can equal to the topological invariant of the gapped systems. This reveals that  $\chi_F$  of normal filled band of the topological SCs exactly determines the numbers of Majorana edge states. We finally show all  $dD$  topological SCs with above properties in different topological classifications and provide the detection scheme of  $\chi_F$  for normal filled band via the average spin structure of topological SCs.

*Generic characterization of Fermi sea topology.*—Our starting point is a  $dD$  metallic system, with electronic dispersion  $E_{\mathbf{k}}$ . Its Fermi sea topology determines the quantization of conductance of this metal and is characterized by the Euler characteristic  $\chi_F$  [13]. For the 1D case,  $\chi_F$  is the number of disconnected components of the Fermi sea. For the higher-dimensional case,  $\chi_F$  is expressed as a summation over the disconnected components of the FSs. The Morse theory [23, 24] provides a direct way to calculate  $\chi_F$  based on the nondegenerate critical points in the filled bands, shown by

$$\chi_F = \sum_m \eta_m. \quad (1)$$

Here  $m$  labels the critical points  $\mathbf{k}_m$  in  $E_{\mathbf{k}}$ , where  $\mathbf{v}_{\mathbf{k}} = \nabla_{\mathbf{k}} E_{\mathbf{k}} = 0$  for  $E_{\mathbf{k}} < E_F$ , with Fermi energy  $E_F$ . The sig-

nature of each critical point is given by  $\eta_m = \text{sgn}(\det \mathbb{H})$ , where  $\mathbb{H}$  is Hessian matrix of  $E_{\mathbf{k}}$  and  $\det \mathbb{H} \neq 0$  hosts that  $\mathbf{k}_m$  are nondegenerate. When a minimum, maximum, or saddle point passes through  $E_F$ , it allows that  $\chi_F$  changes at a Lifshitz transition [25].

However, a generic  $dD$  band dispersion can induce the nonlinear behavior of  $\mathbf{v}_{\mathbf{k}}$  near  $\mathbf{k}_m$ , emerging  $\det \mathbb{H} = 0$  at  $\mathbf{k}_m$ , which characterizes the degenerate critical points. It is clear that Eq. (1) is ill for the degenerate  $\mathbf{k}_m$ . We then give  $\eta_m$  for the degenerate cases by defining an integer topological index

$$\eta_m = \frac{\Gamma(d/2)}{2\pi^{d/2}} \frac{1}{(d-1)!} \int_{\mathcal{L}_m} \hat{\mathbf{v}}_{\mathbf{k}} (d\hat{\mathbf{v}}_{\mathbf{k}})^{d-1} \in \mathbb{Z}, \quad (2)$$

which is the winding number of  $\hat{\mathbf{v}}_{\mathbf{k}} = \mathbf{v}_{\mathbf{k}}/|\mathbf{v}_{\mathbf{k}}|$  around  $\mathbf{k}_m$ . Here ‘d’ denotes the exterior derivative and  $\Gamma(a)$  is  $\Gamma$  function. The counterclockwise contour  $\mathcal{L}_m$  only encloses a single critical point  $\mathbf{k}_m$ . This definition of  $\eta_m$  still keeps  $\chi_F$  to satisfy the Eq. (1), which is known as the Poincaré-Hopf theorem [26]. Moreover, the Eq. (2) can describe the signature of nondegenerate critical points when  $\mathbf{v}_{\mathbf{k}}$  approaches  $\mathbf{k}_m$  linearly. Hence we hereby provide a generic  $\eta_m$  to characterize the nondegenerate and degenerate  $\mathbf{k}_m$  and identify  $\chi_F$ .

To illustrate above results, we take a 2D band dispersion with  $E_{\mathbf{k}} = e_1 e_2 e_3 - \mu$ , where  $e_1 = \sin^2(k_x/2) - \sin^2(k_y/2)$ ,  $e_2 = \sin(k_x/2) \sin(k_y/2)$ , and  $e_3 = m_z - t_s [\cos(k_x/2) + \cos(k_y/2)]$ . Here  $m_z$  is a constant and  $\mu$  is used to shift  $E_F$ . When  $m_z = 0.5t_s$  and  $\mu = 0.18t_s$ , this single band is partially filled and has four hole-like FSs [see Fig. 1(a)]. Meanwhile, both  $v_{1,\mathbf{k}} = 0$  and  $v_{2,\mathbf{k}} = 0$  give fourteen critical points in the band, of which the critical point at  $(k_x, k_y) = (0, 0)$  is degenerate [see Fig. 1(b)]. Based on Eq. (2), we obtain a high-value topological index  $\eta_m = -3$  to characterize it. The remaining critical points are nondegenerate with  $\det \mathbb{H} \neq 0$ , characterized by the positive or negative topological index with unit value [see Fig. 1(c)]. Finally, the topology of the filled Fermi sea is given by  $\chi_F = \sum_m \eta_m = -4$ , which can also be confirmed by the contribution of four hole-like FSs [16]. For the completely filled band,  $\chi_F$  is zero and determined by all critical points in the Fermi sea.

**Reduction of Euler characteristic.**—The topology of Fermi sea can be reduced by using a mapping. Specifically, we firstly map the metallic system to the gapped topological system. By redefining  $v_{0,\mathbf{k}} \equiv E_{\mathbf{k}} - E_F$  and  $\mathbf{v}_{\mathbf{k}} \equiv (v_{1,\mathbf{k}}, v_{2,\mathbf{k}}, \dots, v_{d,\mathbf{k}})$ , we construct a  $dD$  Bloch Hamiltonian with  $\mathbb{Z}$  topological classification,

$$H_{\mathbf{k}} = \sum_{i=0}^d v_{i,\mathbf{k}} \gamma_i. \quad (3)$$

Here  $\gamma$  matrices obey the anticommutation relation and satisfy the trace property  $\text{Tr}[\prod_{i=0}^d \gamma_i] = (-2i)^{d/2}$  (if  $d$  is even) or  $\text{Tr}[\gamma \prod_{i=0}^d \gamma_i] = (-2i)^{(d+1)/2}$  (if  $d$  is odd),

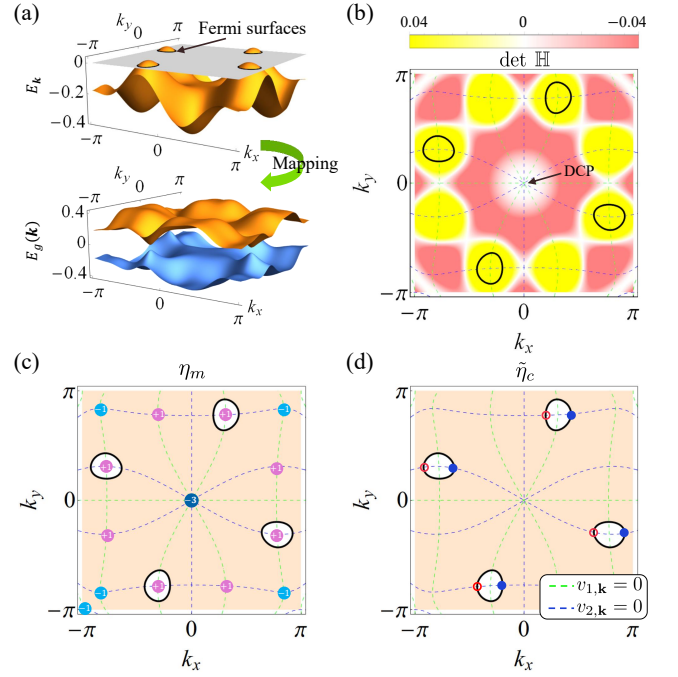


FIG. 1. (a) A 2D filled band  $E_{\mathbf{k}}$  with four hole-like FSs (black curves), which can be translated to two gapped energy bands  $E_g(\mathbf{k})$  by a mapping. (b) Numerical results of  $\det \mathbb{H}$ , where both  $v_{1,\mathbf{k}} = 0$  (green dashed lines) and  $v_{2,\mathbf{k}} = 0$  (blue dashed lines) determine fourteen critical points. Only one critical point at  $(k_x, k_y) = (0, 0)$  is degenerate (DCP) and the others are nondegenerate. (c) Signature of each critical point, characterized by  $\eta_m$ . The topology of filled Fermi sea is captured by  $\mathbf{k}_m$  within the region of  $E_{\mathbf{k}} < E_F$  (orange color), giving  $\chi_F = \sum_m \eta_m = -4$ . (d) The positive (red) or negative (blue) reduced critical points on 1D FSs, where  $\tilde{k}_c$  in the region of  $v_{1,\mathbf{k}_c} < 0$  gives  $\chi_F = \sum_c \tilde{\eta}_c = -4$ . Here solid and open circles indicate  $v_{1,\mathbf{k}_c} < 0$  and  $v_{1,\mathbf{k}_c} > 0$ , respectively.

with  $\gamma = i^{(d+1)/2} \prod_{i=0}^d \gamma_i$ . This ensures that the system only has two energy bands with  $E_g(\mathbf{k}) = \pm \sqrt{\sum_{i=0}^d v_{i,\mathbf{k}}^2}$ , as shown in Fig. 1(a). The gapped  $H_{\mathbf{k}}$  can host the topological phases and characterized by the topological invariant  $\mathcal{W}$ , giving the  $d/2$ -th Chern number (if  $d$  is even) or a  $dD$  winding number (if  $d$  is odd) [3, 27]. One can reduce this  $dD$  topology so that  $\mathcal{W}$  counts the winding of  $\mathbf{v}_{\mathbf{k}}$  on the  $(d-1)D$  momentum subspace of  $v_{0,\mathbf{k}} = 0$ . When employing the topological charge  $\mathcal{C}_m = \frac{\Gamma(d/2)}{2\pi^{d/2}} \int_{\mathcal{L}_m} \frac{1}{|\mathbf{v}_{\mathbf{k}}|^d} \sum_{i=1}^d (-1)^{i-1} v_{i,\mathbf{k}} dv_{1,\mathbf{k}} \wedge \dots \wedge \widehat{dv_{i,\mathbf{k}}} \wedge \dots \wedge dv_{d,\mathbf{k}}$  at each  $\mathbf{k}_m$  [28, 29], it is found that  $\mathcal{W}$  is determined by the summation of topological charges in the regions of  $v_{0,\mathbf{k}} < 0$ , i.e.,

$$\mathcal{W} = \sum_m \mathcal{C}_m. \quad (4)$$

Comparing Eq. (1) and Eq. (4), we observe that  $\chi_F$  exactly equals to  $\mathcal{W}$ , where  $\eta_m$  and FSs of the metallic systems are mapped to  $\mathcal{C}_m$  and  $v_{0,\mathbf{k}} = 0$  in the gapped topo-

TABLE I. The  $\mathbb{Z}$ -classified topological (crystalline) superconductors with the dimensionality  $d = 4n + j$ , where  $j = 1, 2, 3, 4$  and  $n = 0, 1, 2, \dots$ . The BdG Hamiltonian can have time-reversal symmetry ( $T$ ), particle-hole symmetry ( $P$ ), chiral symmetry ( $C$ ), and order-two spatial symmetry ( $S$ ). The superscript of  $S$  indicates the sign of  $S^2$ , and the subscript of  $S$  specifies the commutation (+)/anticommutation (-) relation between  $S$  and  $T$  and/or  $P$ . The fourth column shows the topological classification of  $\mathcal{H}_{\text{BdG}}$ , captured by the zeroth homotopy group of the classifying space.

Dimension	Class	Symmetry	$\pi_0(*)$
$d = 4n + 1$	BDI	$T, P, C$	$\mathbb{Z}$
$d = 4n + 2$	D	$P$	$\mathbb{Z}$
$d = 4n + 3$	DIII	$T, P, C$	$\mathbb{Z}$
$d = 4n + 4$	DIII, CII	$T, P, C, S_{+-}^+ (S_{-+}^-)$	$\mathbb{Z}$
	D, C	$P, S_{-}^+ (S_{+}^-)$	$\mathbb{Z}$

logical systems, respectively. The Lifshitz transitions are also mapped to the topological transitions of  $H_{\mathbf{k}}$ . Actually, Equation (3) tells us that  $E_{\mathbf{k}}$  can firstly be performed band inversion, and then  $\mathbf{v}_{\mathbf{k}}$  acts as a pseudospin-orbit coupling to open its energy gap.

The above  $dD$  gapped band topology can be further reduced to 1D winding number defined by the 1D effective Bloch Hamiltonian  $H_{\tilde{k}} = v_{d-1, \tilde{k}} \tilde{\gamma}_{d-1} + v_{d, \tilde{k}} \tilde{\gamma}_d$ , with  $\tilde{k} \equiv \{\mathbf{k} | v_{0, \mathbf{k}} = \dots = v_{d-2, \mathbf{k}} = 0\}$  and the corresponding Gamma matrices  $\tilde{\gamma}$  [30]. Hence the total topological charges defined by  $H_{\tilde{k}}$  in the regions of  $v_{d-1, \tilde{k}} < 0$  gives  $\mathcal{W} = \sum_c \text{sgn}(\partial v_{d, \tilde{k}} / \partial \tilde{k})$ , of which these topological charges are located at  $\tilde{k}_c \equiv \{\tilde{k} | v_{d, \tilde{k}} = 0\}$ . Following the nontrivial mapping, we finally have

$$\chi_F = \sum_c \frac{(-1)^q}{2} \left[ \text{sgn}(v_{d, \tilde{k}_{c, R}}) - \text{sgn}(v_{d, \tilde{k}_{c, L}}) \right] \quad (5)$$

in the metallic systems, where  $q = 0$  (1) is for the electron-like (hole-like)  $\tilde{k}$ . The subscripts R and L are the right- and left-hand points of  $\tilde{k}_c$ , respectively. Clearly,  $\mathbf{k}_m$  in the  $dD$  system is reduced to  $\tilde{k}_c$  in 1D subsystem, and then we call  $\tilde{k}_c$  as *reduced critical points*. The signature of  $\tilde{k}_c$  is given by  $\tilde{\eta}_c = (-1)^q [\text{sgn}(v_{d, \tilde{k}_{c, R}}) - \text{sgn}(v_{d, \tilde{k}_{c, L}})]/2$ , as shown in Fig. 1(d). Note that these reduced critical points in original BZ are located at  $\mathbf{k}_c \equiv \{\mathbf{k} | v_{0, \mathbf{k}} = \dots = v_{d-2, \mathbf{k}} = v_{d, \mathbf{k}} = 0\}$  and their characterization are different from Ref. [15], in which  $\mathbf{k}_c$  of 2D metallic systems capture the convexity (if  $\partial v_{2, \mathbf{k}} / \partial k_2 > 0$ ) or concavity (if  $\partial v_{2, \mathbf{k}} / \partial k_2 < 0$ ) of FSs. By denoting the number of convex or concave critical points as  $c_e/h$ , the Euler characteristic is given by  $\chi_F = c_e - c_h$ . However,  $\tilde{\eta}_c$  in our theory actually characterizes the 0th Chern number of  $\mathbf{k}_c$  which is determined along 1D FSs. This theory provides an elegant and generic expression to identify  $\chi_F$

via the reduced critical points on FSs.

*Mapping to topological superconductors.*—Mapping the metallic systems to the gapped systems provides a way to identify  $\chi_F$  via the  $\mathbb{Z}$ -classified topological SCs. A single filled band  $E_{\mathbf{k}}$  can perform the band inversion under particle-hole symmetry, and then the nonzero pairing order parameter  $\Delta_{\mathbf{k}}$  can open energy gap. The topological SCs are then emerged and described by Bogoliubov-de Gennes (BdG) Hamiltonian

$$\mathcal{H}_{\text{BdG}}(\mathbf{k}) = \begin{bmatrix} E_{\mathbf{k}} & \Delta_{\mathbf{k}} \\ \Delta_{\mathbf{k}}^\dagger & -E_{\mathbf{k}} \end{bmatrix}. \quad (6)$$

When  $\Delta_{\mathbf{k}}$  have same form with the Fermi velocity  $\mathbf{v}_{\mathbf{k}}$ , the topological invariant  $\mathcal{W}$  of topological SCs can exactly gives  $\chi_F$  of their normal filled band, which has been shown for the special cases [31].

We hereby provide all  $dD$  topological (crystalline) SCs with different topological classifications in Tab. 1, which hosts above special properties. For the simplest four cases of  $d = 1, 2, 3$ , and 4, the normal filled bands and paring order parameters are

$$E_{\mathbf{k}} = -t_s \sum_{i=1}^d \cos k_i - \mu, \quad \Delta_{\mathbf{k}} = (\Delta_0/t_s) \nabla_{\mathbf{k}} E_{\mathbf{k}} \cdot \mathbf{\Gamma}^{(d)}, \quad (7)$$

with  $\mathbf{\Gamma}^{(d)}$  being given by

$$\begin{aligned} \mathbf{\Gamma}_{\text{BDI}}^{(1)} &= -\mathbf{i}, & \mathbf{\Gamma}_{\text{D}}^{(2)} &= (1, -\mathbf{i}), \\ \mathbf{\Gamma}_{\text{DIII}}^{(3)} &= (\sigma_z, -\mathbf{i}\sigma_0, \sigma_x), \\ \mathbf{\Gamma}_{\text{DIII}}^{(4)} &= (\sigma_x \rho_z, -\mathbf{i}\sigma_0 \rho_0, \sigma_x \rho_x, \sigma_z \rho_0), \\ \mathbf{\Gamma}_{\text{CII}}^{(4)} &= (\sigma_x \rho_z, -\mathbf{i}\sigma_0 \rho_0, \sigma_y \rho_0, \sigma_z \rho_0), \\ \mathbf{\Gamma}_{\text{D}}^{(4)} &= (\sigma_z \rho_x, -\mathbf{i}\sigma_0 \rho_0, \sigma_x \rho_x, \sigma_0 \rho_z), \\ \mathbf{\Gamma}_{\text{C}}^{(4)} &= (\sigma_z \rho_x, -\mathbf{i}\sigma_0 \rho_0, \sigma_0 \rho_y, \sigma_0 \rho_z). \end{aligned} \quad (8)$$

These models describe 1D Kitaev chain [32], 2D  $p \pm ip$  superconductor [33], and 3D He-3 B phase [34], respectively. For 4D systems, we seek the topological crystalline SCs with order-two symmetries  $S$  [35]. These models in classes DIII and D have symmetries  $S_{+-}^+ (S_{-+}^-) = \tau_z \sigma_y \rho_y$ ,  $T = \mathbf{i}\sigma_y \mathcal{K}$  and/or  $P = \tau_x \mathcal{K}$ , while  $S_{+-}^+ (S_{-+}^-) = \rho_x$ ,  $T = \mathbf{i}\sigma_y \mathcal{K}$  and/or  $P = \mathbf{i}\tau_x \sigma_z \rho_y \mathcal{K}$  are for classes CII and C. The  $\mathcal{K}$  is a complex conjugate operator. Here  $\sigma$ ,  $\rho$ , and  $\tau$  are Pauli matrices acting on spin, orbit, and Nambu degree of freedom, respectively.

We next show the Fermi sea topology of the normal filled band can be detected in the topological (crystalline) SCs. We employ the Eq. (5) and measure pseudospin polarizations  $\langle \gamma_{i, \mathbf{k}} \rangle = \langle u_{\mathbf{k}} | \gamma_i | u_{\mathbf{k}} \rangle$  with  $i = 0, 1, \dots, d$ , where  $|u_{\mathbf{k}}\rangle$  are ground states of  $\mathcal{H}_{\text{BdG}}$ . Since  $\gamma$  obey the anticommutation relation, we directly have  $\langle \gamma_{i, \mathbf{k}} \rangle = -v_{i, \mathbf{k}}/e_{\mathbf{k}}$  with  $e_{\mathbf{k}} = \sqrt{\sum_{i=0}^d v_{i, \mathbf{k}}^2}$ . Hence these discrete

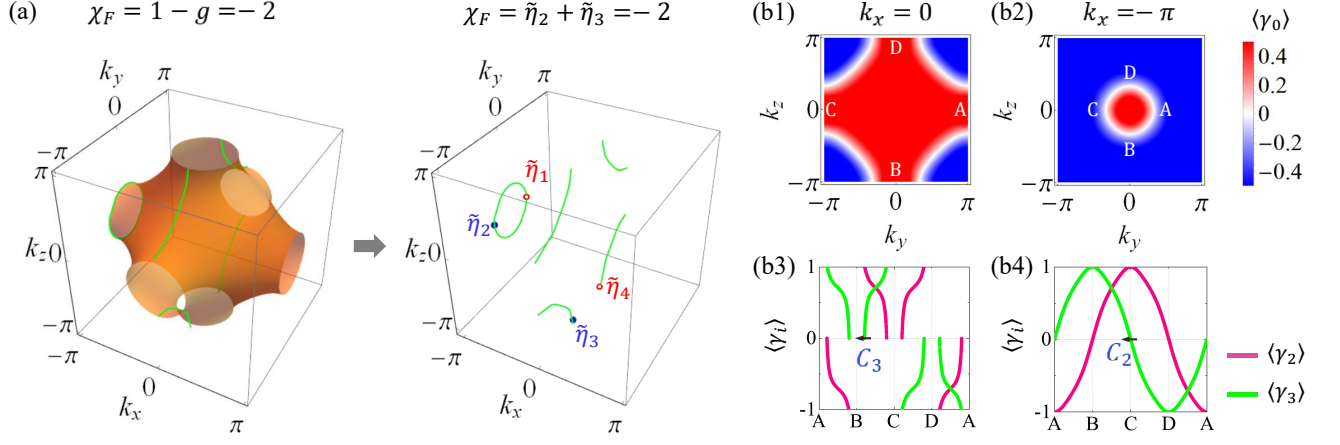


FIG. 2. (a) Reduction of Fermi sea topology in a 3D system. A 2D Fermi surface (orange color) with genus  $g = 3$  gives  $\chi_F = 1 - g = -2$ . Reducing it to obtain 1D curves (green color) on the Fermi surface, denoted as  $\tilde{k}$ , in which the reduced critical points with  $\tilde{\eta}_2$  and  $\tilde{\eta}_3$  determine  $\chi_F = \tilde{\eta}_2 + \tilde{\eta}_3 = -2$ . (b) Measuring the topology of Fermi sea of the normal filled band in a 3D topological superconductor. The pseudospin polarization of  $\langle \gamma_{0,\mathbf{k}} \rangle$  at  $k_x = 0$  in (b1) and  $k_x = -\pi$  in (b2) capture  $\tilde{k}$  by  $\langle \gamma_{0,\mathbf{k}} \rangle = 0$ . The topological charges  $\mathcal{C}_{2,3} = -1$  are determined by  $\langle \gamma_{3,\tilde{k}} \rangle = 0$  and in the regions of  $\langle \gamma_{2,\tilde{k}} \rangle > 0$ , showing in (b3) and (b4). Here we have  $\Delta_0 = t_s$  and  $\mu = -0.5t_s$ .

points  $\mathbf{k}_c$  in FSs are determined by  $\mathbf{k}_c = \{\mathbf{k} | \langle \gamma_{0,\mathbf{k}} \rangle = \dots = \langle \gamma_{d-2,\mathbf{k}} \rangle = \langle \gamma_{d,\mathbf{k}} \rangle = 0\}$ . The reduced critical points are captured by  $\tilde{\eta}_c = (-1)^q [\text{sgn}(\langle \gamma_{d,\mathbf{k}_c,L} \rangle) - \text{sgn}(\langle \gamma_{d,\mathbf{k}_c,R} \rangle)]/2$  in the regions of  $\langle \gamma_{d-1,\mathbf{k}} \rangle > 0$ . The pseudospin polarizations are measurable in realistic quantum simulation experiments and have been applied to identify the topological charges [36–38], providing a possible way for detecting the topology of Fermi sea.

**Numerical results.**—We next provide the numerical results of 3D topological SCs of class DIII to determine  $\chi_F$  of the normal band. The BdG Hamiltonian in the Eq. (7) is explicitly written as  $\mathcal{H}_{\text{BdG}} = E_{\mathbf{k}}\gamma_0 + \Delta_0(\sin k_x\gamma_1 + \sin k_y\gamma_2 + \sin k_z\gamma_3)$  with  $k_{1,2,3} = k_{x,y,z}$ , where  $\gamma_0 = \tau_z$ ,  $\gamma_1 = \tau_x\sigma_z$ ,  $\gamma_2 = \tau_y$ , and  $\gamma_3 = \tau_x\sigma_x$ . Firstly, the FS of normal filled band is figured out by  $E_{\mathbf{k}} = 0$  when  $\mu = -0.5t_s$ , showing a 2D geometry with genus  $g = 3$ . This gives  $\chi_F = 1 - g = -2$  [16], as shown in Fig. 2(a).

By performing reduction, the 1D momentum curves denoted as  $\tilde{k}$  are obtained by  $v_{1,\mathbf{k}} = 0$  on the FS, which are electron-like (hole-like) for  $k_x = 0$  ( $k_x = -\pi$ ). This  $v_{3,\tilde{k}} = 0$  determines four reduced critical points, giving the topological indexes  $\tilde{\eta}_{1,2,3,4}$ , where  $\tilde{\eta}_{2,3}$  are located in regions of  $v_{2,\tilde{k}} < 0$  and which give  $\chi_F = \tilde{\eta}_2 + \tilde{\eta}_3 = -2$ . This is consistent with the result of using the genus of FS to determine  $\chi_F$ . Furthermore, a complete result of  $\chi_F$  depending on  $\mu$  is shown in Fig. 3(a). In the regions of  $-3t_s < \mu < -t_s$  and  $t_s < \mu < 3t_s$ , we have  $\chi_F = 1$ . Yet,  $\chi_F = -2$  is for  $-t_s < \mu < t_s$ . The Lifshitz transition emerges at  $\mu = \pm 3t_s$  and  $\pm t_s$ .

We further show  $\chi_F$  can be detected by the spin textures of topological SCs. By measuring pseudospin polarization of  $\gamma_0$  at  $k_x = 0$  and  $k_x = -\pi$ , the above 1D momentum curves  $\tilde{k}$  are captured by  $\langle \gamma_{0,\mathbf{k}} \rangle = 0$ , as shown in Figs. 2(b1) and 2(b2). We further measure  $\langle \gamma_{2,\tilde{k}} \rangle$  and  $\langle \gamma_{3,\tilde{k}} \rangle$  along  $\tilde{k}$  with the clockwise direction, as shown in Figs. 2(b3) and 2(b4). It is seen that  $\mathcal{C}_{2,3}$  are determined by  $\langle \gamma_{3,\tilde{k}} \rangle = 0$  and in the regions of  $\langle \gamma_{2,\tilde{k}} \rangle > 0$ , where the charge value are identified by  $\mathcal{C}_2 = (\langle \gamma_{3,\tilde{k}_R} \rangle - \langle \gamma_{3,\tilde{k}_L} \rangle)/2 = -1$  and  $\mathcal{C}_3 = (\langle \gamma_{3,\tilde{k}_L} \rangle - \langle \gamma_{3,\tilde{k}_R} \rangle)/2 = -1$ . Hence the Fermi sea topology of the normal filled band is given by  $\chi_F = \mathcal{W} = -2$ , matching with the previous results.

Besides, detecting Majorana edge states is of great significance [39, 40]. For the 3D metallic sample, we can put it on the  $s$ -wave SC and which can be induced as the 3D topological SC by the proximity effect. If the system has a reasonable pairing order and Fermi energy, the numbers of Majorana cone should be given by  $|\chi_F|$ . We numerically calculate the Majorana edge states under the  $z$ -direction open boundary condition, as shown in Fig. 3. Our results may be helpful for the studies of Majorana

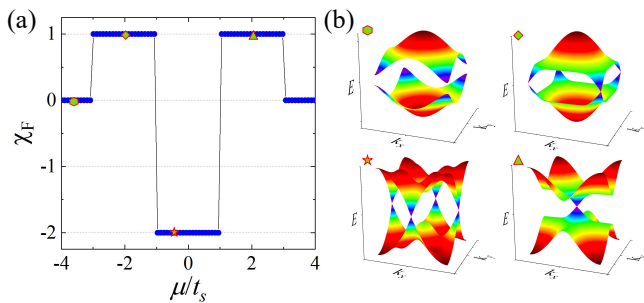


FIG. 3. (a) Numerical results of  $\chi_F$  for the normal band of the 3D topological SC. (b) Majorana edge states for the parameters  $\mu = -3.5t_s, -2t_s, -0.5t_s$ , and  $2t_s$ . The number of Majorana cones is given by  $|\chi_F|$ .

zero modes.

*Discussion and Conclusion.*—The deeply studies of gapped topological phases have driven many novel discoveries, such as fractional charges [41], fractional statistics [42], and non-Abelian statistics [43]. We have established the connection between the Fermi sea topology of metals and the gapped band topology. This nontrivial result may facilitate the discovery of other physical effects caused by the Fermi sea topology in the future. Actually, our reduction for the Euler characteristic origins from the basic idea of dimensional reduction in the gapped band topology [30]. In summary, our generic reduction characterization theory updates the understanding for Fermi sea topology and contribute to its realistic detection. This work shall advance research of quantum topology of metals in both theory and experiments.

We thank Bao-Zong Wang for helpful discussions. This work is supported by the start-up grant of Lanzhou University.

---

\* [jjaw@lzu.edu.cn](mailto:jjaw@lzu.edu.cn)

- [1] K. v. Klitzing, G. Dorda, and M. Pepper, New method for high-accuracy determination of the fine-structure constant based on quantized Hall resistance, *Phys. Rev. Lett.* **45**, 494 (1980).
- [2] D. J. Thouless, M. Kohmoto, M. P. Nightingale, and M. den Nijs, Quantized hall conductance in a two-dimensional periodic potential, *Phys. Rev. Lett.* **49**, 405 (1982).
- [3] M. Z. Hasan and C. L. Kane, Colloquium: topological insulators, *Rev. Mod. Phys.* **82**, 3045 (2010).
- [4] X.-L. Qi and S.-C. Zhang, Topological insulators and superconductors, *Rev. Mod. Phys.* **83**, 1057 (2011).
- [5] R. Landauer, Spatial variation of currents and fields due to localized scatterers in metallic conduction, *IBM J. Res. Dev.* **1**, 223 (1957).
- [6] D. S. Fisher and P. A. Lee, Relation between conductivity and transmission matrix, *Phys. Rev. B* **23**, 6851 (1981).
- [7] M. Büttiker, Four-terminal phase-coherent conductance, *Phys. Rev. Lett.* **57**, 1761 (1986).
- [8] A. D. Stone and A. Szafer, What is measured when you measure a resistance?—The Landauer formula revisited, *IBM J. Res. Dev.* **32**, 384 (1988).
- [9] B. J. Van Wees, H. Van Houten, C. W. J. Beenakker, J. G. Williamson, L. P. Kouwenhoven, D. Van der Marel, and C. T. Foxon, Quantized conductance of point contacts in a two-dimensional electron gas, *Phys. Rev. Lett.* **60**, 848 (1988).
- [10] T. Honda, S. Tarucha, T. Saku, and Y. T. Y. Tokura, Quantized conductance observed in quantum wires 2 to 10  $\mu\text{m}$  long, *Jpn. J. Appl. Phys.* **34**, L72 (1995).
- [11] I. van Weperen, S. R. Plissard, E. P. Bakkers, S. M. Frolov, and L. P. Kouwenhoven, Quantized conductance in an insb nanowire, *Nano Lett.* **13**, 387 (2013).
- [12] S. Frank, P. Poncharal, Z. Wang, and W. A. d. Heer, Carbon nanotube quantum resistors, *Science* **280**, 1744 (1998).
- [13] C. Kane, Quantized nonlinear conductance in ballistic metals, *Phys. Rev. Lett.* **128**, 076801 (2022).
- [14] P. M. Tam, M. Claassen, and C. L. Kane, Topological multipartite entanglement in a Fermi liquid, *Phys. Rev. X* **12**, 031022 (2022).
- [15] P. M. Tam and C. L. Kane, Probing Fermi sea topology by Andreev state transport, *Phys. Rev. Lett.* **130**, 096301 (2023).
- [16] P. M. Tam, C. De Beule, and C. L. Kane, Topological andreev rectification, *Phys. Rev. B* **107**, 245422 (2023).
- [17] P. M. Tam and C. L. Kane, Topological density correlations in a Fermi gas, *Phys. Rev. B* **109**, 035413 (2024).
- [18] F. Yang and H. Zhai, Quantized nonlinear transport with ultracold atoms, *Quantum* **6**, 857 (2022).
- [19] P. Zhang, Quantized topological response in trapped quantum gases, *Phys. Rev. A* **107**, L031305 (2023).
- [20] M. Sato and Y. Ando, Topological superconductors: a review, *Rep. Prog. Phys.* **80**, 076501 (2017).
- [21] T. F. J. Poon and X.-J. Liu, From a semimetal to a chiral fulde-ferrell superfluid, *Phys. Rev. B* **97**, 020501 (2018).
- [22] W. Jia, Z.-H. Huang, X. Wei, Q. Zhao, and X.-J. Liu, Topological superfluids for spin-orbit coupled ultracold fermi gases, *Phys. Rev. B* **99**, 094520 (2019).
- [23] J. W. Milnor, *Morse theory*, Vol. 51 (Princeton University Uress, 1963).
- [24] C. Nash and S. Sen, *Topology and geometry for physicists* (Elsevier, 1988).
- [25] I. M. Lifshitz, Anomalies of electron characteristics of a metal in the high pressure region, *Sov. Phys. JETP* **11**, 1130 (1960).
- [26] F. Dumortier, J. Llibre, and J. C. Artés, *Qualitative theory of planar differential systems*, Vol. 2 (Springer, 2006).
- [27] C.-K. Chiu, J. C. Y. Teo, A. P. Schnyder, and S. Ryu, Classification of topological quantum matter with symmetries, *Rev. Mod. Phys.* **88**, 035005 (2016).
- [28] L. Zhang, L. Zhang, S. Niu, and X.-J. Liu, Dynamical classification of topological quantum phases, *Sci. Bull.* **63**, 1385 (2018).
- [29] L. Zhang, L. Zhang, and X.-J. Liu, Dynamical detection of topological charges, *Phys. Rev. A* **99**, 053606 (2019).
- [30] W. Jia, L. Zhang, L. Zhang, and X.-J. Liu, Dynamically characterizing topological phases by high-order topological charges, *Phys. Rev. A* **103**, 052213 (2021).
- [31] F. Yang, X. Li, and C. Li, Euler-Chern correspondence via topological superconductivity, *Phys. Rev. Research* **5**, 033073 (2023).
- [32] A. Y. Kitaev, Unpaired Majorana fermions in quantum wires, *Physics-Uspekhi* **44**, 131 (2001).
- [33] C. Kallin and J. Berlinsky, Chiral superconductors, *Rep. Prog. Phys.* **79**, 054502 (2016).
- [34] A. J. Leggett, A theoretical description of the new phases of liquid He 3, *Rev. Mod. Phys.* **47**, 331 (1975).
- [35] K. Shiozaki and M. Sato, Topology of crystalline insulators and superconductors, *Phys. Rev. B* **90**, 165114 (2014).
- [36] W. Ji, L. Zhang, M. Wang, L. Zhang, Y. Guo, Z. Chai, X. Rong, F. Shi, X.-J. Liu, Y. Wang, and J. Du, Quantum simulation for three-dimensional chiral topological insulator, *Phys. Rev. Lett.* **125**, 020504 (2020).
- [37] X.-L. Yu, W. Ji, L. Zhang, Y. Wang, J. Wu, and X.-J. Liu, Quantum dynamical characterization and simulation of topological phases with high-order band inversion surfaces, *Phys. Rev. X Quantum* **2**, 020320 (2021).
- [38] J. Niu, T. Yan, Y. Zhou, Z. Tao, X. Li, W. Liu, L. Zhang,

- H. Jia, S. Liu, Z. Yan, Y. Chen, and D. Yu, Simulation of higher-order topological phases and related topological phase transitions in a superconducting qubit, *Sci. Bull.* **66**, 1168 (2021).
- [39] L. Fu and C. L. Kane, Superconducting proximity effect and majorana fermions at the surface of a topological insulator, *Phys. Rev. Lett.* **100**, 096407 (2008).
- [40] F. Wilczek, Majorana returns, *Nat. Phys.* **5**, 614 (2009).
- [41] R. B. Laughlin, Quantized Hall conductivity in two dimensions, *Phys. Rev. B* **23**, 5632 (1981).
- [42] F. Wilczek, Remarks on dyons, *Phys. Rev. Lett.* **48**, 1146 (1982).
- [43] X.-G. Wen, Non-Abelian statistics in the fractional quantum Hall states, *Phys. Rev. Lett.* **66**, 802 (1991).